*Manuscript
Click here to view linked References

publisher version with DOI: https://doi.org/10.1016/j.surfcoat.2019.125017

Deposition of thin films containing carboxylic acid groups on polyurethane foams by atmospheric pressure non-equilibrium plasma jet

Dr. Vincenza Armenise[a], Prof. Antonella Milella [a,b], Prof. Francesco Fracassi[a,b], Dr. Piera Bosso[a], Dr. Fiorenza Fanelli[b,*],

[a]*Department of Chemistry, University of Bari "Aldo Moro", via Orabona 4, 70126 Bari, Italy*

[b]*Institute of Nanotechnology (NANOTEC), National Research Council (CNR), c/o Department of Chemistry, University of Bari "Aldo Moro", via Orabona 4, 70126 Bari, Italy*

* Corresponding authors at:

Institute of Nanotechnology (NANOTEC), National Research Council, c/o Department of Chemistry, University of Bari "Aldo Moro", via Orabona 4, 70126 Bari, Italy.

E-mail address: fiorenza.fanelli@cnr.it (F. Fanelli).

Phone: +39 0805442227, *Fax:* +39 0805443405

Abstract

Thin films containing carboxylic acid groups are deposited on open-cell polyurethane (PU) foams by using an atmospheric pressure non-equilibrium plasma jet, in dielectric barrier discharge configuration, fed with helium, acrylic acid and ethylene.

The arrangement of the plasma jet, the sample holder, and the substrate is carefully optimized to enable the penetration of the plasma ejected from the remote source throughout the three-dimensional (3D) porous structure of the foam, and, therefore, to achieve the uniform coverage of the entire substrate.

X-ray photoelectron spectroscopy analyses and scanning electron microscopy observations confirm that both the outer and the inner surfaces of the foam can be functionalized with the plasma-deposited coating, showing moderate changes in surface chemical composition and coating thickness moving from the exterior to the interior of the plasma-treated samples.

The ability of the foams to adsorb heavy metals from water is tested through evaluation of cadmium ions (Cd^{2+}) removal. The foams adsorption capacity can increase more than 10 times after plasma deposition and remains unchanged over 8 adsorption-release cycles.

Keywords

atmospheric pressure plasma jet

thin film deposition

acrylic acid

open-cell foam

3D porous material

1. Introduction

The deposition of coatings containing carboxylic acid (COOH) groups using non-equilibrium plasmas has been extensively investigated for many possible applications. Relevant examples in the literature on both low pressure (LP) and atmospheric pressure (AP) plasma processing include the enhancement of the adhesion between polymers and metal films [1-3], the improvement of the adsorption capacity of carbon black granules for basic compounds in liquid and gas phase [4], the increase of the ability of carbon nanotubes to adsorb heavy metal ions from aqueous solutions [5,6], the enhancement of protein attachment as well as of cell adhesion and proliferation on surfaces for biomedical applications [7-11], the increase of the pervaporation efficiency of polymeric membranes [12].

Among the different precursors enabling plasma deposition of thin films bearing COOH functional groups [7,13,14], acrylic acid (AA) has been the most frequently employed [7]. Recently, its utilization has received renewed attention in deposition processes exploiting many different atmospheric pressure plasma sources [9-11,15-23]. Indeed, AP plasma technology represents nowadays a new avenue for surface processing of materials with reduced costs and easy-to-handle apparatuses [24,25]. Interestingly, a wide range of atmospheric pressure plasma jets (APPJs), typically fed with a noble gas (i.e., helium and argon) and AA vapors, were utilized for various purposes, i.e., for the treatment of PP membranes to be used as separators in lithium-ion batteries [2], to modify the surface of fluorocarbon polymers for metal adhesion improving [16], to coat polydimethylsiloxane layers for biomedical and microfluidic applications [22], for the surface modification of silk fibers in order to immobilize antimicrobial peptides [18]. As far as the optimization of the coating chemical composition is concerned, various studies pointed out that highly functionalized polymeric layers can be obtained by injecting the AA aerosol in the downstream region of APPJ devices [9,23]. On the other hand, it is widely acknowledged that a severe disadvantage for the practical use of the deposits obtained with plasmas fed by AA is

their poor stability in water and humid environment, which commonly results in delamination and preferential removal of COOH groups [7,21,26]. Few publications deal with this important issue and/or with the improvement of the water stability of coatings obtained by AA in AP plasmas. In a recent study carried out by Bosso et al. [21], a plasma jet with dielectric barrier discharge (DBD) electrode configuration (hereinafter referred to as "DBD jet") fed with mixtures of helium, AA and ethylene was utilized to deposit water stable thin films on flat two-dimensional (2D) substrates. Specifically, the plasma copolymerization (also named codeposition) of AA and ethylene was exploited to improve the stability of the coatings upon water immersion. It is, in fact, acknowledged that unsaturated hydrocarbon (e.g., ethylene, 1,7-octadiene, styrene) when utilized as comonomers can act as crosslinkers and/or chain-extenders, eventually leading to thin films containing COOH groups characterized by good stability in water. Bosso et al. [21] demonstrated the chemical and morphological stability of the coatings obtained from acrylic acid/ethylene codeposition upon immersion in water for 72 h. In particular, chemical derivatization in conjunction with XPS revealed a negligible decrease of the surface concentration of COOH groups after water immersion.

In this work, the plasma process reported in the above discussed publication was exploited to deposit COOH-containing thin films on three-dimensional (3D) open-cell polyurethane (PU) foams. PU foams are characterized by good resistance to acidic and alkaline solutions, low water absorption, thermal stability up to 180° C, adequate mechanical strength, and are suitable for several advanced applications, provided that they are properly functionalized [27-29]. Application-oriented studies reported, for instance, on the utilization of functionalized PU foams as catalytic materials [30], chemical sensors [31], and sorbent materials for trace metal preconcentration [28,29] and oil/water separation [32]. Nowadays, the surface functionalization of 3D porous materials is a very important issue in AP plasma processing [33-37] due to the possible applications in several technological fields [8,32,33,37,38]. For

this purpose, the utilization of AP plasma jets (APPJs) is in principle particularly advantageous, since the remote operation allows placing the substrate outside the source physical boundaries, making the surface modification of complex 3D material easier [25]. To date, few studies have addressed the APPJ processing of complex porous materials (e.g., foams and scaffold) [34,39] with special focus on penetration of the plasma treatment into the sample interior. Interestingly, in case of the He/O_2 APPJ plasma treatment of poly-ε-caprolactone (PCL) porous scaffolds, Trizio et al. [34] reported the evolution of the O/C XPS atomic ratios measured on sections of the scaffold as a function of the distance from the top surface. Higher O/C ratios were detected at the top surface and the sub-surface regions with respect to the bulk. The gradient of the chemical composition through the scaffolds attested for the limited penetration and reaction of the plasma species within the interior of the material. This example suggests that additional effort should be directed to obtain an enhancement of the penetration of the plasma into the porous material and, therefore, to achieve uniform modification of both the outer and inner surfaces of the substrates. In this regards, it is worth noting that to our best knowledge, no studies on APPJ deposition on 3D porous materials has been published so far.

The main scope of this study is to cover the entire 3D porous structure of PU foams, with coatings containing COOH groups by using an AP DBD plasma jet fed by He, AA and ethylene. For this purpose, different spatial arrangements of the APPJ, the sample holder, and the substrate were tested in order to promote plasma penetration inside the foam pores. XPS and SEM analyses allowed evaluating the overall uniformity of the plasma treatment on the entire sample in terms of surface chemistry and morphology, respectively. Since carboxylic groups can act as binding sites for heavy metal ions [5,6,40,41] the utilization of the plasma-functionalized foam as adsorbent for cadmium ions in water solution was evaluated.

2. Material and methods

The deposition processes were carried out using an APPJ with coaxial cylindrical DBD configuration (Fig. 1), as described previously in full detail [21]. The DBD jet consists of an inner high voltage (HV) cylindrical electrode (stainless steel, 2 mm diameter), a dielectric tube (Pyrex glass, 6 mm inner diameter, 1.5 mm thickness, 75 mm length) and an external tubular electrode (stainless steel, 9 mm inner diameter, 50 mm length) connected to ground (GND). The discharge ignites in the 2 mm thick annular channel between the HV electrode and the dielectric tube [21,25]. The latter projects 5 mm beyond the lower edge of the electrodes, therefore the plasma source is characterized by a circular outlet (9 mm diameter). For safety reasons, the APPJ is located into an unsealed (i.e., open to air) Plexiglas chamber slightly pumped by a diaphragm pump, to allow the exhaust gas to be drawn away during the deposition processes carried out at atmospheric pressure.

The DBD was generated by applying to the electrodes a 20 kHz sinusoidal high voltage of 1.4 kV_{RMS}. The applied voltage was measured by means of a HV probe (Tektronix P6015A), while the current flowing through the circuit was determined by measuring the voltage drop (Tektronix P2200 voltage probe) across a 50 Ω resistor connected in series with the grounded electrode. Measurements were processed to calculate the average power dissipated by the discharge as the integral of the product of voltage and current values over one cycle, divided by the period.

The discharge was fed with a helium (Air liquide, 99.99%), acrylic acid (2-propenoic acid, Sigma-Aldrich, 99%), and ethylene (C_2H_4, Airliquide, 99.95%) mixture. The gas flow rates were controlled by MKS electronic mass flow controllers, whereas AA vapours were admitted in the DBD jet by a He stream bubbling through a liquid AA reservoir kept at 30°C (Fig. 1) [21]. Before each plasma process, the feed mixture was allowed homogenizing for 10 min, also to reduce air contamination inside the plasma source as well as in the environment surrounding the device outlet. Deposition processes were performed using a helium (i.e., main

or dilution gas) flow rate of 7 slm (standard liter per minute), and AA and ethylene concentrations of 22 ppm and 200 ppm, respectively.

The sample holder, located below the jet outlet, is provided with a computer-controlled xy translational stage, which enables the sample xy-displacement during the plasma processes and, therefore, the enlargement of the sample area interested by the deposition. A commercial open-cell PU foam (Angst + Pfister) characterized by polyester polyol-based polyurethane structure, a pore density of 45 pores per inch (ppi) and porosity of about 97% was utilized as substrate in the form of 4 mm thick rectangular strips, having length and width of 50 mm and 20 mm, respectively. In deposition processes, the foam strips were scanned under the plasma source by using the track-by-track displacement scheme [42] reported in Fig. 1b (x-displacement, Δx = 50 mm; x-speed = 5 mm·s^{-1}; y-displacement, Δy = 4 mm; y-speed = 3 mm·s^{-1}). The displacement scheme was repeated for a total process duration of 103.5 min, corresponding to an average deposition time per unit area of the sample of 10.35 min·cm^{-2}. Borosilicate glass slides (Agar scientific) and CaF_2 substrates (Crystan) were also utilized for characterization purposes. The above mentioned track-by-track displacement scheme and the total process duration of 103.5 min were employed for all deposition processes carried out in this work on both flat substrates and PU foam samples.

Four different arrangements of the DBD jet, the PU foam and the sample holder were utilized to improve the uniformity of thin film deposition on the porous substrates (Fig. 2). For the sake of clarity, the explored setup configurations are described in full detail in the next section; broadly, they exploit:

(i) two different sample holders: either a 0.635 mm thick alumina (Al_2O_3) plate or a grounded electrode covered with a 0.635 mm thick Al_2O_3 plate;

(ii) two different source-to-substrate distances, (i.e, the distance between the source outlet and the upper surface of the foam): either 3 mm or 5 mm;

(iii) sample positioning either in direct contact with the sample holder or suspended 1 mm above the sample holder by using 1 mm thick glass spacers.

XPS analyses were carried out using a PHI P5000 VersaProbe II scanning XPS microprobe spectrometer equipped with a monochromatic Al Kα X-ray source (1486.6 eV). The utilization of a X-ray beam induced secondary electron imaging (SXI) system enabled the confident location of the analyzed spots on foam struts. Fig. S1 reports the typical secondary electron image of the PU foam acquired with the SXI system, obtained by scanning the X-ray beam over the sample (minimum x-ray beam size of less than 7.5 μm). XPS spectra were collected using a X-ray beam spot size of 100 μm (power of 24.5 W) at a location corresponding to the center of the SXI image. Survey (0-1200 eV) and high resolution spectra (C 1s, O 1s, N 1s, Si 2p) were recorded in fixed analyzer transmission (FAT) mode at a pass energy of 117.40 eV and 46.95 eV, respectively, and at a take-off angle of 45° respect to the sample normal. Dual-beam charge neutralization was constantly applied during analysis. Charge correction of the spectra was performed by taking the hydrocarbon component (C-C/C-H) of the C 1s high resolution spectrum as internal reference (binding energy, BE = 284.8 eV). The surface atomic concentrations and curve-fitting of the high resolution C 1s spectra were obtained using the MultiPak software (Version 9.5.0.8, 30-10-2013, Ulvac-PHI, Inc.). A nonlinear Shirley background subtraction algorithm was utilized. Five peaks were used for the C 1s curve-fitting, centred at 284.8 ± 0.2 eV (C-C, C-H), 285.7± 0.2 eV (C-N), 286.5 ± 0.2 eV (C-O), 288.1 ± 0.2 eV (O-C-O, C=O) and 289.1 ± 0.2 eV (COOH, COOR and urethane functionalities) [17,21,32]. The full-width at half maximum (FWHM) of each C 1s component was allowed to vary between 1.3-1.6 eV. XPS analyses were repeated on two samples produced in different experiments; each sample was analysed at three different positions (three analysed points per position) corresponding to the top, bottom and cross-section of the foam strip. The inner surfaces of 3D substrates (i.e., foam

cross-section) were analysed by cutting the foams strips with a scalpel blade perpendicularly to the strip top.

Fourier-transform infrared (FTIR) absorption spectra of coating deposited on CaF_2 substrates were acquired using a vacuum Bruker Vertex 70v FTIR spectrometer in the range 375-4000 cm^{-1} over 32 scans with a resolution of 4 cm^{-1}. After baseline correction, spectra were normalized to most intense absorption in the 1500-1700 cm^{-1} region.

A Zeiss SUPRA 40 field emission scanning electron microscope (FESEM) was used to investigate the morphology of PU foams and to estimate the thickness of the deposited thin films. SEM images were acquired with a Everhart–Thornley detector at the working distance in the range 7-8.5 mm, electron acceleration voltage (extra-high tension, EHT) of 3.00 kV, magnification in the range 0.15-100 k×. Before SEM observation the substrates were sputter-coated with 20 nm of Cr utilizing a turbo-pumped sputter coater (Quorum Technologies, model Q150T). Cross-sectional SEM analyses were performed after sample freezing in liquid N_2 for 120 s and cutting with a scalpel blade perpendicularly to the foam strip top. The observation of cross-sectioned ligaments allowed to appreciate the presence of the coating deposited on the foam and to determine its thickness by using the "point-to-point measure" function of Zeiss SmartSEM software. Mean coatings thickness values and associated uncertainties are obtained averaging over thirty measurements per each analysed position on the foam substrate (i.e., foam top, cross-section and bottom). To assess statistically significant differences between the mean thickness values the Student's t-test was used. In particular data were compared by using a two-sided t-test for unpaired samples, while the level of significance was set to 0.05 (confidence level of 95%).

The thickness of the coating deposited on flat glass samples was determined by stylus profilometry. After deposition the coating was partially scratched off the sample with a scalpel and the thickness was measured by a using Dektak XT Bruker stylus profiler. Mean

coating thickness values and associated uncertainties are obtained averaging results from three different samples produced in different experiments (12 measurements on each sample).

The ability of PU foams to adsorb heavy metal ions from water solutions was evaluated by means of Anodic Stripping Voltammetry (ASV) analyses carried out using a Metrhom 757 VA Computrace polarograph. Cadmium (Standard for AAS, Sigma-Aldrich) was used as metal ion probe and its concentration in test solution was evaluated before and after the immersion of 0.05 g of foam in 20 mL of 500 ppb (4.45 μmol/L) solution, under continuous stirring. The determination was performed in differential pulse ASV mode, using a classical three-electrode cell composed by a hanging mercury drop electrode as working electrode, an Ag/AgCl reference electrode with saturated 3 mol/L KCl, and a platinum wire counter electrode. An acetate buffer solution (Fluka) was added to test solution deaerated with N_2 (Air liquid) for 100 s. Electrochemical deposition was performed at -0.8 V for 90 s under stirring, then the stirring was switched off and the curve was recorded in the potential range -1.15 to -0.22 V (sweep rate of 0.059 V/s). A Cd^{2+} standard solution was added to the cell to quantify the metal ions concentration. The adsorption capacity was expressed as micromoles of cadmium ions removed per gram of adsorbent foam (μmol/g). Reported adsorption capacity values are the average of determinations on three solutions (3 determinations per solution) obtained with three different foams.

3. Results and discussion

Fig. 2 reports the four different setup configurations employed in the deposition processes to enable plasma penetration into the interior of the porous samples and, in turn, to improve the overall uniformity of the surface modification. Specifically, the configurations reported in Fig. 2 and utilized in this work present different spatial arrangements of the DBD jet, the foam substrate and the sample holder:

- configuration a (Fig. 2a) in which the source-to-sample distance is 5 mm, an alumina plate is utilized as sample holder, and the foam strip is placed in direct contact with the sample holder;
- configuration b (Fig. 2b), differing from configuration a only in the utilization of a grounded electrode underneath the alumina plate;
- configuration c (Fig. 2c) in which the source-to-sample distance is 3 mm and the foam strip is suspended 1 mm above the alumina plate;
- configuration d (Fig. 2d), showing an analogous arrangement to that of configuration c, with the only difference of presenting a grounded electrode underneath the alumina plate.

Figs. 2e-h show the photographs of the different setup configurations during thin film deposition. First of all, both Figs. 2e and 2g, corresponding respectively to configurations a and c (Figs. 2a,c), allow clearly appreciating that, when the alumina plate is used as sample holder, the plasma exiting the APPJ device predominantly spreads on the top surface of the PU foam sample. Differently, Figs. 2f and 2h demonstrate that the utilization of dielectric-covered grounded electrode as sample holder (i.e., configurations b and d in Figs. 2b,d) promotes plasma penetration into the porous sample. In particular, in case of configuration d (suspended foam sample, Fig. 2d) plasma clearly develops also in the 1 mm thick "free" gap between the bottom surface of the foam and the sample holder (Fig. 2h). It is worth noting that, in spite of these significant changes in plasma development and appearance, only a very slight increase of the average power dissipated by the discharge in observed when the grounded electrode is added (i.e., 2.00 ± 0.05 W for configurations a and c, 2.20 ± 0.05 W for configurations b and d).

In connection with these outcomes, attention should be drawn to the recent literature on strategies that can be utilized to favor the propagation of the plasma exiting APPJs devices (i.e., the so-called "plasma plume") through the external environment. For instance, it has been shown that the electric and gas flow fields can act synergistically to enhance the

propagation and characteristics of the plasma plume [25,43], eventually leading to more effective surface treatment [25,43-45]. In particular, in case of APPJs with linear-field configuration (i.e., having parallel electric and flow fields) intensification and improved propagation of the plasma plume is observed compared to cross-field configuration APPJs (i.e., having electric field perpendicular to the feed flow field) [43]. Interestingly, the DBD jet utilized in this work presents a cross-field configuration, the electric field being in radial direction and gas flowing in axial direction. However, the introduction of a dielectric-covered grounded electrode in front of the source outlet allows realizing a mixed cross-field/linear-field configuration and, therefore, enables plasma development throughout the porous sample.

Interestingly, in all the different setup configurations utilized in the deposition processes (Figs. 2a-d) it is possible to observe a considerable spreading of the plasma on the PU foam samples (Figs. 2e-h). In particular, while the DBD jet has a circular outlet with a diameter of 9 mm, the plasma spreads on the foam surface over a circular region with diameter in the range 18-24 mm when the source-to-sample distance is 5 mm (configurations a and b, Figs. 2e,f). Even increased spreading of the plasma (circular region with diameter in the range of 26-30 mm) is observed for configurations c and d (Figs. 2g,h) characterized by a reduced source-to-sample distance of 3 mm. Considering the track-by-track sample displacement scheme utilized during deposition (Fig. 1b), it is worth noting that due to plasma spreading on the sample transverse overlapping of treated tracks is obtained (i.e., transverse overlapping of treated areas) and this is expected to lead to a complete and more uniform coverage of the porous sample by the plasma-deposited layer [25,42].

To assess the uniformity of the surface functionalization, XPS and SEM analyses were carried out at three different positions on the plasma-treated foam strips (Fig. 3a, showing as example configuration d), i.e., on the outer surface directly exposed to the plasma exiting the device (top), in the center of the porous substrate (cross-section) and on the bottom surface facing the

Al_2O_3 plate (bottom). Table 1 reports the XPS surface atomic concentrations of PU foams plasma coated using the various setup configurations of Fig. 2; data for the pristine foam and for plasma-coated glass substrates are also reported for comparison. Results for the pristine foam show that the carbon, oxygen, nitrogen, and silicon surface atomic concentrations are about 74, 20.5, 4.5 and 1 at %, respectively. The presence of a low surface atomic concentration of silicon (Si 2p signal centered at about 102.5 eV) is very likely due to residual silicone-based surfactants [46] utilized in the preparation process of the commercial foam. On the other hand, thin films deposited on flat glass substrates present carbon and oxygen atomic percentages of about 74 and 26 at %, respectively, with negligible differences between results obtained in two deposition configuration (i.e., configuration a and b). Considering the plasma-coated foams using configurations a and c (i.e, presenting as sample holder the alumina plate without the grounded electrode, Figs. 2a,c), it can be appreciated that the top side of the sample exhibits a surface chemical composition similar to the one obtained for the coated glass samples. However, moving to the cross-section and bottom side of the foam sample (i.e., with increasing the distance from the foam top surface and, in turn, from the APPJ outlet) some nitrogen is also revealed. This could suggest a non-uniform coverage of the sample and/or a low coating thickness (close to the sampling depth of XPS, i.e., 4-10 nm). In contrast, when configurations b and d are employed (i.e., grounded underneath the dielectric alumina plate), XPS atomic percentages determined on the top, bottom and inner surfaces of the foam, are very similar, they differ from those reported for the pristine foam and agree with measurements on plasma-coated glass samples (Table 1). Interestingly, thin film deposition seems to occur on the bottom of the foam strips also in case of configuration b, where the sample is placed in direct contact with the dielectric-covered grounded electrode. In fact, as it can be observed in Table 1, in case of the bottom side of the foam strip plasma-coated using configuration b, the surface chemical composition evaluated by XPS is very

similar to that observed for the coated glass samples and the thickness of the deposited coating is 80 ± 20 nm.

This could be explained considering that, due to the complex structure of the material, the foam contact with the dielectric plate is only possible at some protruding ligaments. Therefore, the discharge (spreading on the dielectric plate surface Fig.2b) and/or depositing species can reach approximately the entire bottom surface of the substrate.

The curve-fitting results of the high-resolution XPS C 1s signals (Table 2 and Fig. 3) show that in case of the plasma-treated foam (Fig. 3b) the surface atomic concentration of the component due to carboxylic acidic and ester groups (COOH and COOR) at 289.1 ± 0.2 eV increases with respect to the pristine foam (Fig. 3c). It is worthy specifying that in case of the untreated sample this component also includes contributions from the urethane and ester functionalities of the polyester-type polyurethane material (Fig. S2 reports the FTIR spectrum of the pristine PU foam) [35]. In addition, curve-fitting results in Table 2 highlight the high uniformity of the surface chemistry of the porous substrates treated with configuration d as well as the very similar surface composition respect to the plasma polymer deposited on the glass slide (for comparison purpose, Fig. S3 reports the typical XPS C 1s signal from adventitious carbon on the untreated glass slide).

The FTIR spectrum of the thin film deposited on a CaF_2 substrate is reported in Fig. 4. The most important features are: (i) the broad OH stretching band (3700-2300 cm^{-1}) due to both carboxylic acid and alcoholic moieties, (ii) the superimposed CH_x stretching absorptions (3000-2800cm^{-1}), (iii) the broad band (2640 cm^{-1}) due to the combined low frequency vibrations of C-O and O-H in both carboxylic acid and alcoholic groups enhanced by Fermi resonance with the fundamental OH stretching vibration, (iv) the C=O stretching peak (1715 cm^{-1}), (v) the CH_x bending absorptions (1500-1350 cm^{-1}). The complex shape of the OH stretching band and the absorptions at about 2640 cm^{-1} and 1715 cm^{-1} are evidence of the presence of COOH groups confirming the deposition of a coating functionalized with these

acidic groups [21]. This outcome well agrees with the literature on characteristic infrared absorptions of poly(acrylic acid) [47].

Interestingly, no changes in chemical composition of the coatings were observed by FTIR and XPS analyses after ageing for 12 months under ambient conditions.

Representative SEM images of the pristine and plasma-coated foams using configuration d are reported in Fig. 5. The low-magnification SEM image in Fig. 5a shows the open-cell porous structure of the foam (pore dimension in the range 300-1000 μm) consisting of a 3D network of interconnected ligaments (minimum width in the range 80-150 μm). The observation of cross-sectioned ligaments allowed the measurement of the thickness of the deposited coating (indicated by the white arrows in Figs. 5b and S4) at different positions of the PU foams (i.e., top, bottom and cross-section, Fig. 3a). For instance, SEM images reported in Fig. S4 allow appreciating the presence of the coating (thickness in the range 100-180 nm) at different positions of the porous sample plasma coated using configuration d. The high-magnification SEM image in Fig. 5c clearly shows the presence of a smooth and uniform coating on the surface of the plasma-treated foam (condition d, Fig. 2d) as compared with the pristine foam (Fig. 5d). Average thickness values of the coatings deposited on the PU foams using the various setup configurations are reported in Table 1. First of all, a statistically significant increase (t-test, level of significance of 0.05) of the coating thickness can be observed when the sample holder includes the grounded electrode underneath the alumina plate (configurations b and d). This evidence indicates that the addition of the grounded electrode favors the transport of thin film precursors towards the substrate [25]. This increase can be better appreciated in case of the flat glass (Table 1). As expected, thicker coatings are deposited on the glass samples as compared to the foams, and this can be ascribed to the complex geometry the porous samples. Moreover, considering coating thickness non-uniformity over the entire plasma-treated porous samples (Table 1), t-test results indicate that the differences between the mean thickness values obtained at the three positions

analysed on each plasma-treated foams(i.e. top, cross-section and bottom) are statistically significant for all the treated foams samples, except for the foam plasma coated by using configuration d. Therefore it can be concluded that the optimal configuration that allows obtaining the thickest deposit with the best chemical and thickness uniformity corresponds to configuration d (Fig. 2d), in which the APPJ-to-sample distance is set to 3 mm, a dielectric-coated grounded electrode is utilized as sample holder and the PU foam is suspended 1 mm above the substrate holder, to enable adequate plasma development also under the sample.

The PU foams plasma coated using the configuration d (Fig. 2d) were utilized to investigate the adsorption of cadmium ions from aqueous solution. Since the deposits contained acidic carboxylic groups, after the foams immersion in the Cd^{2+} solution a pH decrease was detected. Therefore, in order to perform the adsorption experiments under controlled conditions, the pH was corrected with NaOH solution. It is worth mentioning that immersion of the pristine foam in the Cd^{2+} solution did not cause any pH change.

The effect of the pH of the Cd^{2+} cadmium solution on the adsorption capacity of the pristine and the plasma-treated PU foams is presented in Fig. 6a. At pH 5 the adsorption capacity of treated foam is quite similar to that of pristine one, then it increases with the pH. Indeed, at pH 7 the plasma-treated foam exhibits an adsorption capacity 12 times greater than that of the pristine sample. The adsorption improvement with pH is reasonably due to the dissociation of COOH groups of the deposited coating, which develop the negative charge responsible for the interaction with cadmium positive ions [5,48,49]. It is worth specifying that adsorption tests were not carried out at pH greater than 8 for two main reasons: (i) the chemical state of the dissolved metal changes [6,49], (ii) thin film decomposition occurs. The effect of the immersion time in adsorption experiments is reported in Fig. 6b; a rather steep increase of the adsorption capacity can be observed with the immersion time and a plateau is reached in 30 min. The recyclability of the functionalized PU foam as heavy metal adsorbent was evaluated over up to 8 adsorption-desorption cycles. The release of cadmium ions was obtained by

immersing the foam an acidic solution (HCl solution, pH 2) for 60 min, under continuous stirring. The obtained results are shown in Fig. 6c and allow appreciating that the performance of plasma-treated foams remains unchanged within the experimental uncertainty also after 8 adsorption-desorption.

4. Conclusion

In this work, thin films containing carboxylic acid groups were deposited on 3D open-cell PU foams by using an AP plasma jet in DBD configuration fed with helium, acrylic acid and ethylene. Various alternative setup configurations were proposed and investigated, corresponding to different spatial arrangements of the DBD jet, the sample holder, and the porous substrate.

XPS and SEM analyses allowed identifying the best setup configuration to obtain uniform thin film deposition on both the exterior and interior of the foam. It was found that the utilization of an alumina-covered grounded electrode as sample holder favors plasma penetration into the porous materials; moreover, when the substrate is suspended above the sample holder (no direct contact) plasma development under the sample is also promoted. This, in conjunction with sample displacement, enables the uniform coverage of the porous samples. Interestingly, the deposition process increased the ability of the foam to adsorb heavy metal ions from water. A good recyclability was achieved; in fact, any appreciable reduction of the adsorption capacity for cadmium ions was not detected over 8 adsorption-release cycles.

Supplementary Material

Typical secondary electron image of the PU foam acquired with the X-ray beam induced secondary electron imaging (SXI) system of the XPS spectrometer; attenuated total

reflection-FTIR spectrum of the pristine PU foam; XPS C 1s signal of the untreated glass substrate; additional SEM images showing the coating deposited on the foam struts.

Acknowledgements

Domenico Benedetti, Danilo Benedetti and Savino Cosmai are gratefully acknowledged for the skillful technical assistance. This research was supported by the Italian Ministry for Education, University and Research (MIUR) under grants PONa3_00369 and PON01_02239. The financial support of Regione Puglia Regione Puglia, under grants "LIPP" (grant no. 51, within the Framework Programme Agreement APQ "Ricerca Scientifica", II atto integrativo - Reti di Laboratori Pubblici di Ricerca) and "ATTIV'AZIONE" (grant code S8R8930, call "Aiuti a Sostegno Cluster Tecnologici Regionali"), is also acknowledged.

References

[1] J. Friedrich, R. Mix, R.-D. Schulze, A. Rau, Ultra-Thin polymer layer deposition by aerosol–Dielectric Barrier Discharge (DBD) and Electrospray Ionization (ESI) at atmospheric pressure, J. Adhes. Sci. Technol. 24 (2010) 1329–1350.

[2] M. Yin, J. Huang, J. Yu, G. Chen, S. Qu, X. Wang, C. Li, The polypropylene membrane modified by an atmospheric pressure plasma jet as a separator for lithium-ion button battery, Electrochim. Acta 260 (2018) 489–497.

[3] F. Addou, T. Duguet, P. Bosso, A. Zhang, E. Amin-Chalhoub, F. Fanelli, C. Vahlas, Metallization of carbon fiber reinforced polymers: chemical kinetics, adhesion, and properties, Surf. Coat. Technol. 308 (2016) 62–69.

[4] N. De Vietro, R. d'Agostino, F. Fracassi, Improvement of the adsorption properties of carbon black granules by means of plasma enhanced-chemical vapour deposition with acrylic acid vapours, Carbon 49 (2011) 249–255.

[5] H. Cheng, J. Yu, K. Zeng, G. Hou, Application of poly(acrylic acid)-multiwalled carbon nanotube composite for enrichment of Trace Hg(II), Plasma Process. Polym. 10 (2013) 931–937.

[6] H. Chen, J. Li, D. Shao, X. Ren, X. Wang, Poly(acrylic acid) grafted multiwall carbon nanotubes by plasma techniques for Co(II) removal from aqueous solution, Chem. Eng. J. 210 (2012) 475–481.

[7] R. Bitar, P. Cools, N. De Geyter, R. Morent, Acrylic acid plasma polymerization for biomedical use, Appl. Surf. Sci. 448 (2018) 168–185.

[8] P. Cools, H. Declercq, R. Ghobeira , R. Morent, N. De Geyter, Acrylic acid plasma coatings for enhanced cell migration in PCL 3D additive manufactured scaffolds ,Surf. Coat. Technol. 350 (2018) 925–935.

[9] O. Carton, D. B. Salem, S. Bhatt, J. Pulpytel, F. Arefi-Khonsari, Plasma polymerization of acrylic acid by atmospheric pressure nitrogen plasma jet for biomedical applications, Plasma Process. Polym. 9 (2012) 984–993.

[10] M. Donegan, D.P. Dowling, Protein adhesion on water stable atmospheric plasma deposited acrylic acid coatings, Surf. Coat. Technol. 234 (2013) 53–59.

[11] L.S. Dolci, S.D. Quiroga, M. Gherardi, R. Laurita, A. Liguori, P. Sanibondi, A. Fiorani, L. Calzà, V. Colombo, M. L. Focarete, Carboxyl surface functionalization of poly(L-lactic acid) electrospun nanofibers through atmospheric non-thermal plasma affects fibroblast morphology, Plasma Process. Polym. 11 (2014) 203–213.

[12] D.E. Weibel, C. Vilani, A.C. Habert , C.A. Achete, Surface modification of polyurethane membranes using RF-plasma treatment with polymerizable and non-polymerizable gases, Surf. Coat. Technol. 201 (2006) 4190–4194.

[13] B.R. Pistillo, L. Detomaso, E.Sardella, P.Favia, R.d'Agostino, RF-plasma deposition and surface characterization of stable (COOH)-rich thin films from cyclic L-lactide, Plasma Process. Polym. 4 (2007) S817–S820.

[14] W.-Y. Chen, A. Matthews, F.R. Jones, K.-S. Chen, Immobilization of carboxylic acid groups on polymeric substrates by plasma-enhanced chemical vapor or atmospheric pressure plasma deposition of acetic acid, Thin Solid Films 666 (2018) 54–60.

[15] L.J. Ward, W.C.E. Schofield, J.P.S. Badyal, Atmospheric pressure plasma deposition of structurally well-defined polyacrylic acid films, Chem. Mater. 15 (2003) 1466–1469.

[16] M. Okubo, M. Tahara, T. Kuroki, T. Hibimo, N. Saeki, Plating technology for fluorocarbon polymer films using atmospheric-pressure non-thermal plasma graft polymerization, J. Photopolym. Sci. Technol. 21 (2008) 219–224.

[17] R. Morent, N. De Geyter, S. Van Vlierberghe, E. Vanderleyden, P. Dubruel, C. Leys, E. Schacht, Deposition of polyacrylic acid films by means of an atmospheric pressure dielectric barrier discharge, Plasma Chem. Plasma Process. 29 (2009) 103–117.

[18] G. Chen, M. Zhou, Z. Zhang, G. Lv, S. Massey, W. Smith, M. Tatoulian, Acrylic acid polymer coatings on silk fibers by room-temperature APGD plasma jets, Plasma Process. Polym. 8 (2011) 701–708.

[19] C. Amorosi, T. Fouquet, V. Toniazzo, D. Ruch , L. Averous , V. Ball, M. Michel, Growth rate, morphology, chemical composition and oligomerization state of plasma polymer films made from acrylic and methacrylic acid under dielectric barrier discharge, React. Funct. Polym. 72 (2012) 341–348.

[20] F. Moix, K. McKay, J.L. Walsh, J.W. Bradley, Atmospheric-pressure plasma polymerization of acrylic acid: gas-phase ion chemistry, Plasma Process. Polym. 13 (2016) 236–240.

[21] P. Bosso, F. Fanelli, F. Fracassi, Deposition of water-stable coatings containing carboxylic acid groups by atmospheric pressure cold plasma jet, Plasma Process. Polym. 13 (2016) 217–226.

[22] M. Bashir, S. Bashir, H.U. Khan, Deposition of polyacrylic acid films on PDMS substrate in dielectric barrier corona discharge at atmospheric pressure, Surf. Interf. Anal. (2018) 1–10.

[23] W.-Y. Chen, A. Matthews, F. R. Jones, K.-S. Chen, Deposition of a stable and high concentration of carboxylic acid functional groups onto a silicon surface via a tailored remote atmospheric pressure plasma process, Surf. Coat. Technol.336 (2018) 67–71.

[24] F. Massines, C. Sarra-Bournet, F. Fanelli, N. Naudé, N. Gherardi, Atmospheric pressure low temperature direct plasma technology: status and challenges for thin film deposition, Plasma Process. Polym. 9 (2012) 1041–1073.

[25] F. Fanelli, F. Fracassi, Atmospheric pressure non-equilibrium plasma jet technology: general features, specificities and applications in surface processing of materials, Surf. Coat. Technol. 322 (2017) 174–201.

[26] M. Vandenbossche, D. Hegemann, Recent approaches to reduce aging phenomena in oxygen- and nitrogen-containing plasma polymer films: an overview, Curr. Opin. Solid State Mater. Sci. 22 (2018) 26–38.

[27] S.W. Myung, Y.H. Yeom, Y.M. Jang, H.S. Choi, D. Cho, Preparation of a reticulated polyurethane foam grafted with poly(acrylic acid) through atmospheric pressure plasma treatment and its lysozyme immobilization, J. Mater. Sci. Mater. Med. 16 (2005) 745–751.

[28] V.A. Lemos, M.S. Santos, E.S. Santos, M.J.S. Santos, W.N.L. dos Santos, A.S. Souza, D.S. de Jesus, C.F. das Virgens, M.S. Carvalho, N. Oleszczuk, M.G.R. Vale, B. Welz, S.L.C. Ferreira, Application of polyurethane foam as a sorbent for trace metal pre-concentration — A review, Spectrochim. Acta Part B 62 (2007) 4–12.

[29] N. Burham, Separation and preconcentration system for lead and cadmium determination in natural samples using 2-aminoacetylthiophenol modified polyurethane foam, Desalination 249 (2009) 1199–1205.

[30] E. Pardieu, N.T.T. Chau, T. Dintzer, T. Romero, D. Favier, T. Roland, D. Edouard, L. Jierry, V. Ritleng, Polydopamine-coated open cell polyurethane foams as an inexpensive, flexible yet robust catalyst support: a proof of concept, Chem. Commun. 52 (2016) 4691–4693.

[31] Y. Wang, G. A. Sotzing, R. A. Weiss, conductive polymer foams as sensors for volatile amines, Chem. Mater. 15 (2003) 375-377.

[32] J. Ge, H. Zhao, H. Zhu, J. Huang, L. Shi, S.Yu, Advanced sorbents for oil-spill cleanup: recent advances and future perspectives; Adv. Mater. 28 (2016) 10459–10490.

[33] L.L. Gonçalves Da Silva, L.G. Ferreira, A. Lima Santos, E. Cocchieri Botelho, A. Tóth, K.G. Kostov, Treatment of reticulated vitreous carbon by dielectric barrier discharge plasma for electrodes production, IEEE Trans. Plasma Chem. 41 (2013) 3207–3213.

[34] I. Trizio, F. Intranuovo, R. Gristina, G. Dilecce, P. Favia, He/O_2 Atmospheric pressure plasma jet treatments of PCL scaffolds for tissue engineering and regenerative medicine, Plasma Process. Polym. 12 (2015) 1451–1458.

[35] F. Fanelli, F. Fracassi, Thin film deposition on open-cell foams by atmospheric pressure dielectric barrier discharges, Plasma Process. Polym. 13 (2016) 13, 470–479.

[36] F. Fanelli, P. Bosso, A.M. Mastrangelo, F. Fracassi, Thin film deposition at atmospheric pressure using dielectric barrier discharges: advances on three-dimensional porous substrates and functional coatings, Jpn. J. Appl. Phys. 55 (2016) 07LA01.

[37] M. Michlíček, A. Manakhov, E. Dvořáková, L. Zajíčková, Homogeneity and penetration depth of atmospheric pressure plasma polymerization onto electrospun nanofibrous mats, Appl. Surf. Sci. 471 (2019) 835–841.

[38] H. Zhang, W.J. Suszynski, K.V. Agrawal, M. Tsapatsis, S. Al Hashimi, L.F. Francis, Coating of open cell foams, Ind. Eng. Chem. Res. 51 (2012) 9250–9259.

[39] C.X. Wang, Y.P. Qiu, Two sided modification of wool fabrics by atmospheric pressure plasma jet: influence of processing parameters on plasma penetration, Surf. Coat. Technol. 201 (2007) 6273–6277.

[40] S. Duan, X. Liu, Y. Wang, Y. Meng, A. Alsaedi, T. Hayat, J. Li, Plasma surface modification of materials and their entrapment of water contaminant: a review, Plasma Process Polym. (2017) e1600218.

[41] N. Chitpong, S.M. Husson, Polyacid functionalized cellulose nanofiber membranes for removal of heavy metals from impaired waters, J. Membrane Sci. 523 (2017) 418–429.

[42] C. Merten, C. Regula, A. Hartwig, J. Ihde, R. Wilken, Track by track: the structure of single tracks of atmospheric pressure plasma polymerized hexamethyldisiloxane (HMDSO) analyzed by infraredmicroscopy, Plasma Process. Polym. 10 (2013) 60–68.

[43] J.L. Walsh, M.G. Kong, Contrasting characteristics of linear-field and cross-field atmospheric plasma jets, Appl. Phys. Lett. 93 (2008) 111501.

[44] X. Li, J. Li, J. Chu, P. Zhang, and P. Jia, A linear-field plasma jet for generating a brush-shaped laminar plume at atmospheric pressure, Phys. Plasmas 23 (2016) 063521.

[45] R. Zhou, B. Zhang, R. Zhou, F. Liu, Z. Fang, K. Ostrikov, Linear-field plasma jet arrays excited by high-voltage alternating current and nanosecond pulses, J. Appl. Phys. 124 (2018) 033301.

[46] M.L. Pinto, J. Pires, A.P. Carvalho, M.B. de Carvalho, J.C. Bordado, Sorption Isotherms of Organic Vapors on Polyurethane Foams, J. Phys. Chem. B 108 (2004), 13813–13820.

[47] J. Dong, Y. Ozaki, K. Nakashima, infrared, raman, and near-infrared spectroscopic evidence for the coexistence of various hydrogen-bond forms in poly(acrylic acid), Macromolecules, 30 (1997) 1111–1117.

[48] M. Karakıskla, The adsorption of Cu(II) ion from aqueous solution upon acrylic acid grafted poly(ethylene terephthalate) fibers, J. Appl. Polym. Sci. 87 (2003) 1216–1220.

[49] V.C. Srivastava, I.D. Mall, I.M. Mishra, Competitive adsorption of cadmium (II) and nickel (II) metal ions from aqueous solution onto rice husk ash, Chem.l Engin. Process. 48 (2009) 370–379.

Table 1. XPS surface atomic concentrations of the pristine PU foam and of the glass and foam samples coated by APPJ using the different setup configurations investigated in this work (Fig. 2). Thickness of the coatings deposited on glass and foam samples. Measurements are taken at different positions on the plasma-treated foam substrates as illustrated in Fig. 3a. Configuration a: source-to-sample distance of 5 mm, alumina plate as sample holder, foam strip in direct contact with the sample holder; configuration b: source-to-sample distance of 5 mm, grounded electrode covered by an alumina plate as sample holder, foam strip in contact with the sample holder; configuration c: source-to-sample distance of 3 mm, alumina plate as sample holder, foam strip suspended 1 mm above the sample holder; configuration d: source-to-sample distance of 3 mm, grounded electrode covered by an alumina plate as sample holder, foam strip suspended 1 mm above the sample holder.

Sample/deposition configuration	Position	C (at %)	O (at %)	N (at %)	Si (at %)	Coating thickness (nm)
Pristine foam	-	74.0 ± 4.0	20.5 ± 1.0	4.5 ± 0.5	1.0 ± 0.2	-

Glass slide/a	-	74.5 ± 0.5	25.5 ± 0.5	-	-	340 ± 40
Glass slide/b	-	72.8 ± 0.5	27.2 ± 0.5	-	-	910 ± 90
Foam/a	Top	74.5 ± 0.6	25.5 ± 0.6	-	-	90 ± 20
	Cross-section	73.0 ± 0.7	26.0 ± 0.6	1.0 ± 0.6	-	80 ± 20
	Bottom	72.1 ± 1.1	25.0 ± 0.9	2.3 ± 0.6	0.6 ± 0.4	50 ± 15
Foam/b	Top	74.0 ± 0.5	26.0 ± 0.5	-	-	140 ± 50
	Cross-section	73.8 ± 1.4	26.2 ± 1.4	-	-	100 ± 20
	Bottom	74.0 ± 0.5	26.0 ± 0.8	-	-	100 ± 30
Foam/c	Top	76.0 ± 1.0	24.0 ± 1.0	-	-	110 ± 30
	Cross-section	75.5 ± 1.5	23.5 ± 0.5	1.0 ± 1.0	-	80 ± 20
	Bottom	75.5 ± 1.5	23.0 ± 0.5	1.5 ± 1.0	-	80 ± 20
Foam/d	Top	73.4 ± 0.5	26.6 ± 0.5	-	-	140 ± 40
	Cross-section	73.1 ± 0.8	26.9 ± 0.8	-	-	120 ± 20
	Bottom	73.2 ± 0.5	26.8 ± 0.5	-	-	130 ± 30

Table 2. Curve-fitting results of the high resolution XPS C1s spectra of the pristine foam, the plasma-coated foam (configuration d) and the plasma-coated glass slide (configuration b). Spectra are taken at different position on the plasma-treated foam substrate as illustrated in Fig. 3a (i.e., top, cross-section and bottom of the foam strip).

Sample	**Position**	**C-C, C-H (at %)**	**C-N (at %)**	**C-O (at %)**	**C=O, O-C-O (at %)**	**COOH, COOR (at %)**
Pristine PU foam	---	44.5 ± 1.5	4.0± 0.4	19.5 ± 1.5	-	6.0 ± 0.4
PU foam-coating	Top	47.1 ± 0.4	-	13.4 ± 0.2	4.0 ± 0.4	8.9 ± 0.3
	Cross-section	46.3 ± 1.8	-	13.9 ± 0.4	3.9 ± 0.5	9.0 ± 0.3
	Bottom	46.4 ± 0.7	-	13.4 ± 1.0	4.0 ± 1.0	9.4 ± 0.4
Glass slide-coating	---	45.8 ± 0.9	-	14.4 ± 0.2	4.2 ± 0.3	8.4 ± 0.2

Figure captions

Fig. 1. (a) Schematic representation of the plasma reactor, (b) track-by-track sample displacement scheme utilized during the plasma processes to deposit thin films on 4 mm thick

PU foam strips with length and width of 50 mm and 20 mm, respectively (Δx = 50 mm; x-speed = 5 mm·s^{-1}; Δy = 4 mm; y-speed = 3 mm·s^{-1}).

Fig. 2. Various setup configurations utilized in this work for thin film deposition and, specifically, exploiting different spatial arrangements of the plasma jet, the foam substrate and the sample holder: (a) configuration a: source-to-sample distance of 5 mm, alumina plate as sample holder, foam strip in direct contact with the sample holder; (b) configuration b: source-to-sample distance of 5 mm, grounded electrode covered by an alumina plate as sample holder, foam strip in contact with the sample holder; (c) configuration c: source-to-sample distance of 3 mm, alumina plate as sample holder, foam strip suspended 1 mm above the sample holder; (d) configuration d: source-to-sample distance of 3 mm, grounded electrode covered by an alumina plate as sample holder, foam strip suspended 1 mm above the sample holder. Photographs of the different setup configurations during thin film deposition: (e) configuration a, (f) configuration b, (g) configuration c, (h) confinguration d.

Fig. 3. (a) Schematic representation showing the different positions analyzed by XPS and SEM on the plasma-treated foams and, specifically, the foam strip top, bottom and cross-section (i.e. center of the porous sample after sample cutting with a scalpe blade); as example, configuration d is reported (Fig. 2d). High resolution XPS C 1s spectra of (b) the pristine foam, (c) the plasma-coated foam (configuration d) and (d) plasma-coated glass sample (configuration b).

Fig. 4. FTIR spectrum of the coating deposited on a flat CaF_2 substrate.

Fig.5. SEM images of the plasma-coated foam showing the porous structure of the sample (a) and a cross-sectioned ligament where the deposited coating is clearly visible and indicated by

white arrows (b). High-magnification SEM images of the plasma-coated (c) and pristine (d) foam. SEM images of the foam treated by using configuration d are reported (Fig. 2d).

Fig. 6. (a) Effect of the pH on the cadmium adsorption capacity of the pristine PU foam and of the plasma-treated foam (immersion time of 60 min). (b) Effect of the immersion time in cadmium solution (pH 7) on the adsorption capacity of the plasma-treated PU foam. (c) Recyclability of the plasma-treated PU foam evaluated for adsorption tests performed using a cadmium solution at pH 7 and an immersion time of 60 min per adsorption cycle. Reported data refer the foam treated by using configuration d (Fig. 2d).

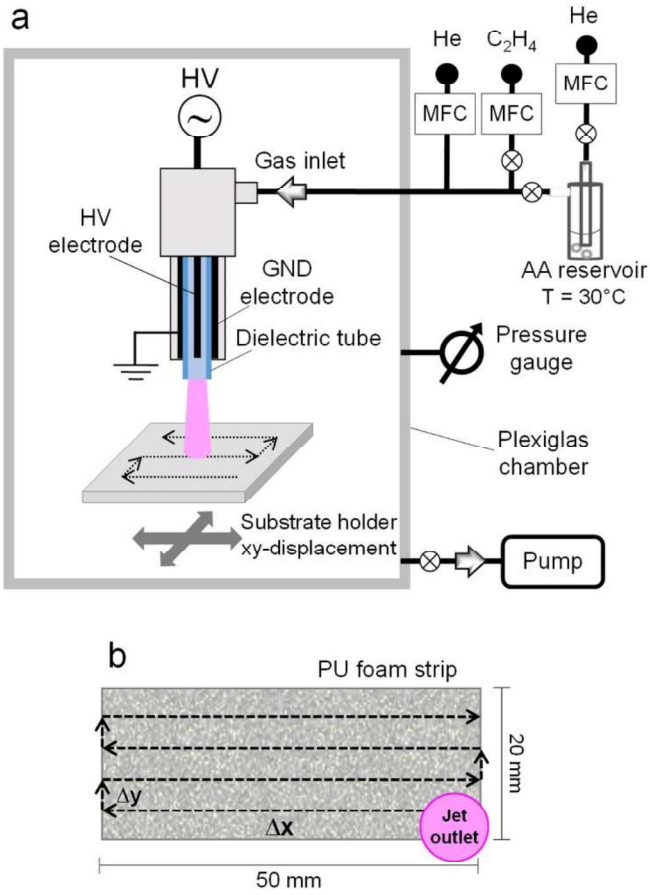

Fig. 1 (color online only)

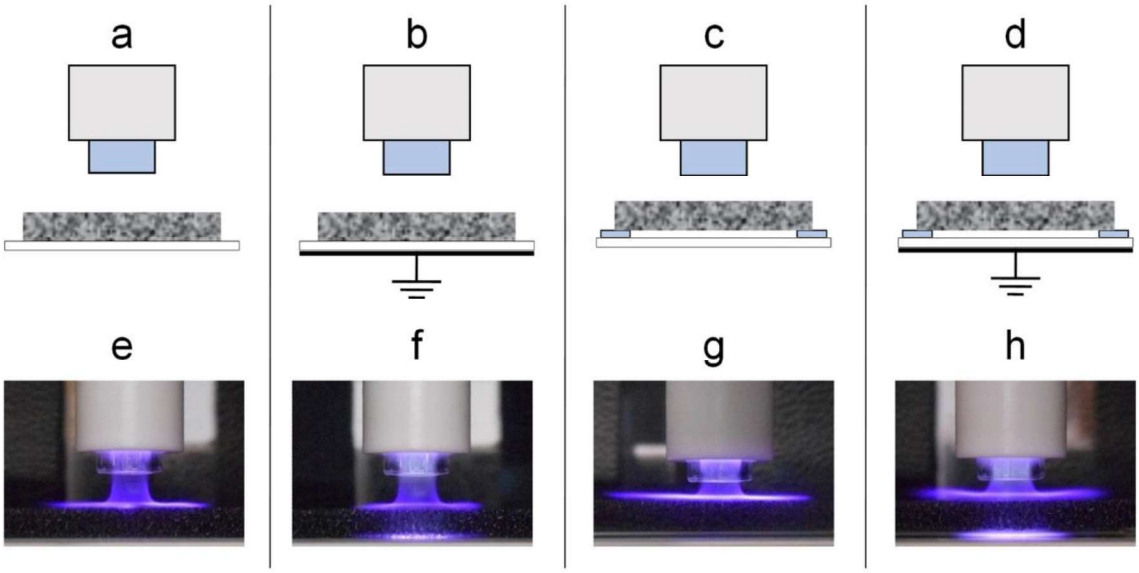

Fig. 2 (color online only)

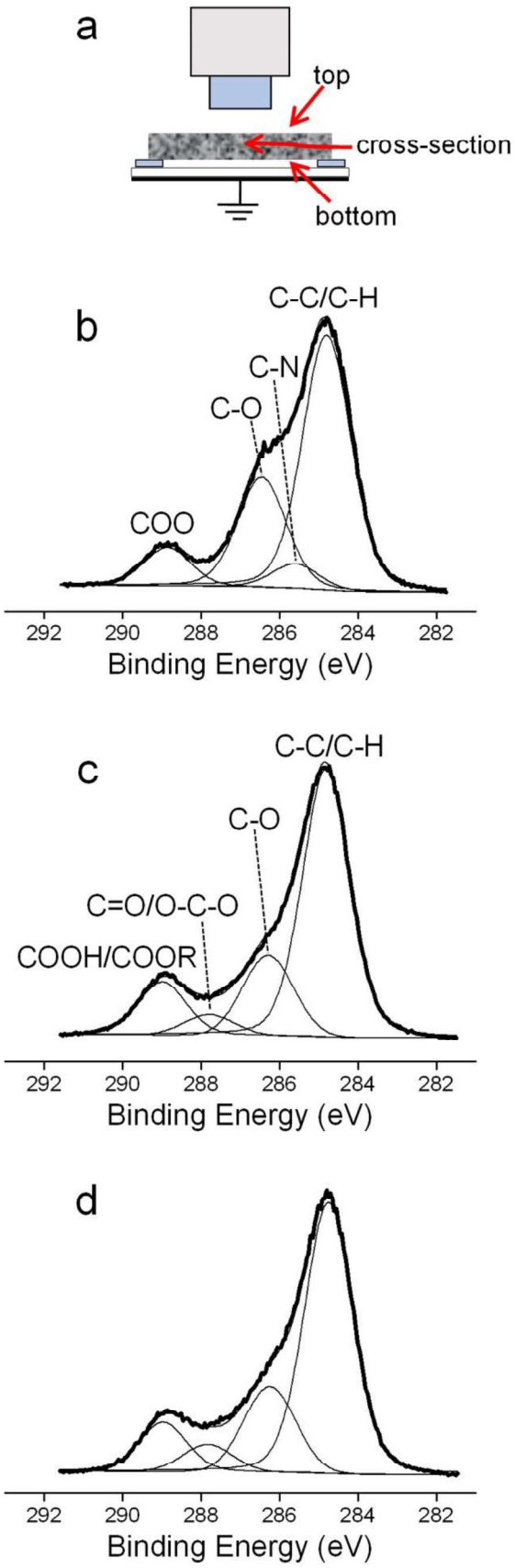

Fig. 3 (color online only)

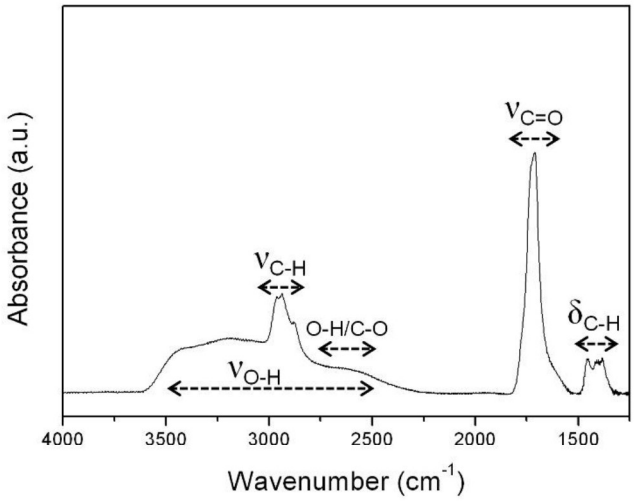
Absorbance (a.u.)
$\nu_{C=O}$
ν_{C-H}
O-H/C-O
δ_{C-H}
ν_{O-H}
4000
3500
3000
2500
2000
1500
Wavenumber (cm^{-1})

Fig. 4

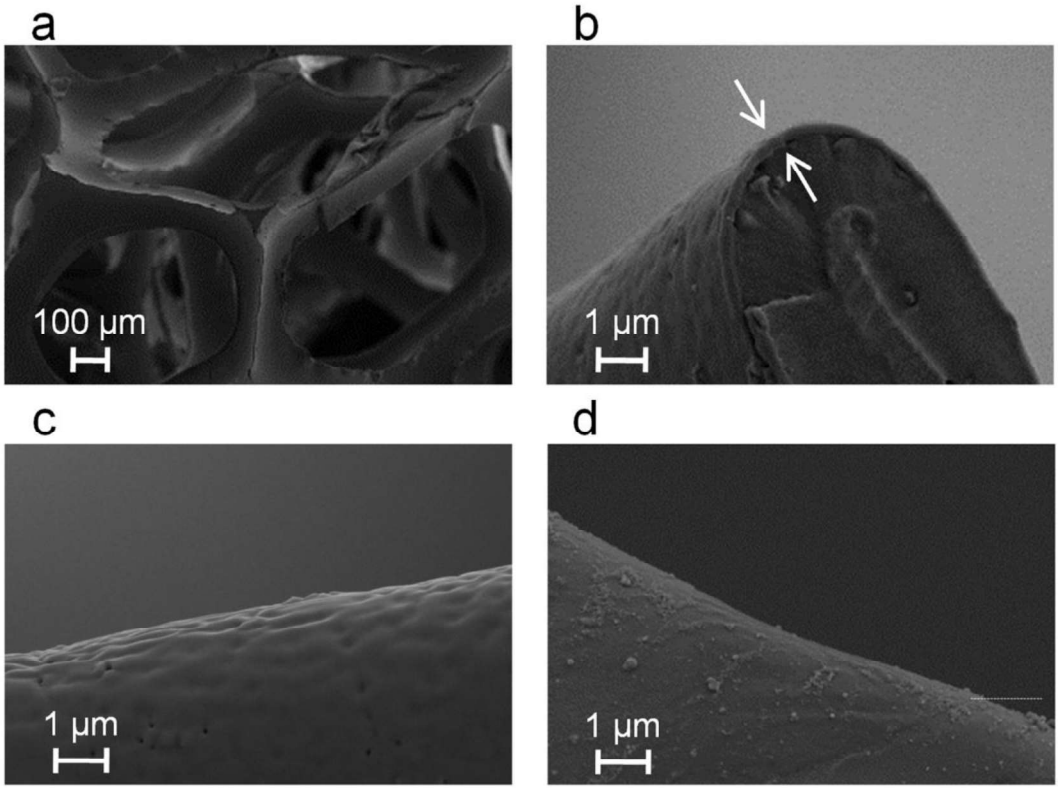

Fig. 5

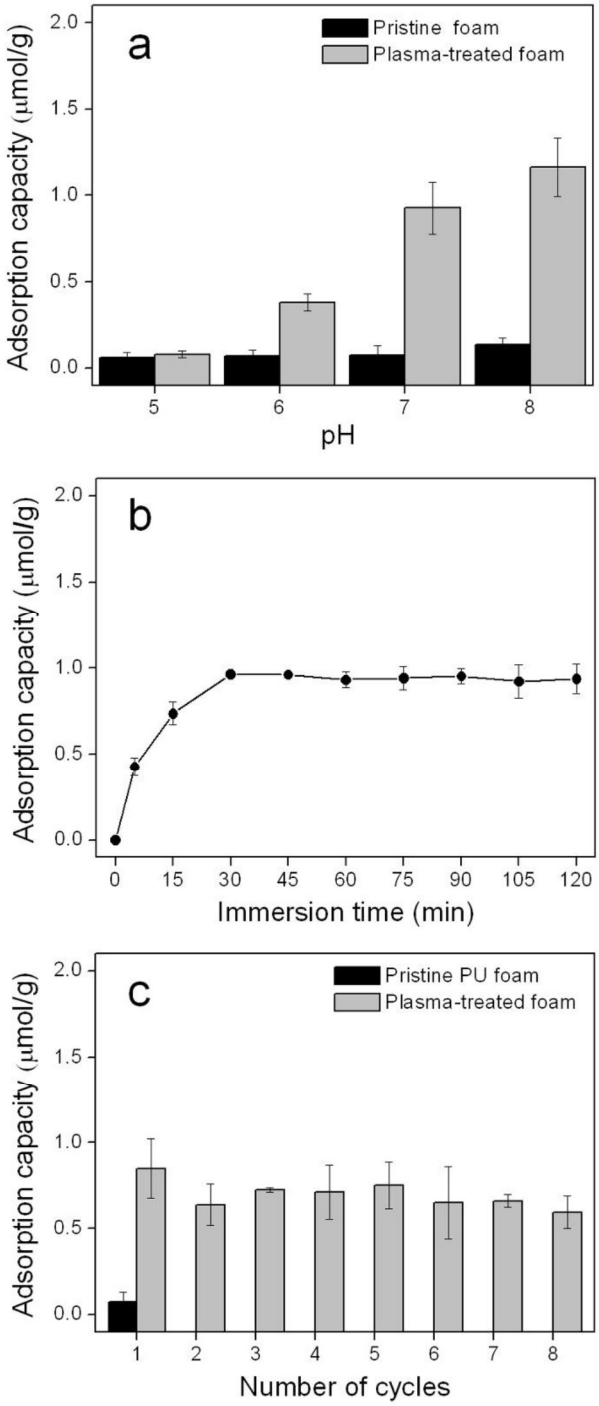
a
Pristine foam
Plasma-treated foam
Adsorption capacity (μmol/g)
2.0
1.5
1.0
0.5
0.0
5
6
7
8
pH
b
Adsorption capacity (μmol/g)
0
15
30
45
60
75
90
105
120
Immersion time (min)
c
Pristine PU foam
Plasma-treated foam
Adsorption capacity (μmol/g)
1
2
3
4
5
6
7
8
Number of cycles

Fig. 6

Graphical abstract